Arabian Journal of Chemistry (2022) **15**, 103936

King Saud University

Arabian Journal of Chemistry

www.ksu.edu.sa
www.sciencedirect.com

ORIGINAL ARTICLE

Application of synergistic β-lactamase inhibitors and antibiotics in the treatment of wounds infected by superbugs

Xiaoyuan Ding [a,1], Jing Su [b,1], Xiao Chen [c], Shizhong Zhang [c], Mengkao Li [c], Jie yang [a], Zekun Wang [a], Jingyuan Wang [a], Weiyun Wang [a], Dongdong Sun [a,*], Guojun Wang [c,*]

[a] *School of Life Sciences, Anhui Agricultural University, Hefei 230036, Anhui, P.R. China*
[b] *Department of Geriatric Cardiovascular, Taian City Central Hospital, Taian, Shandong 271000, China*
[c] *Department of Neurosurgery, Taian City Central Hospital, Taian, Shandong 271000, China*

Received 13 January 2022; accepted 17 April 2022
Available online 22 April 2022

KEYWORDS

Prussian blue;
β-lactamase inhibitor;
Amoxicillin;
Antibacterial action;
Antibiotic resistance

Abstract Amoxicillin appears to be clinically drug-resistant due to the presence of β-lactamase in bacteria. Here, we designed and prepared a hollow Prussian Blue (HPB)-based therapeutic nanoplatform that was constructed by encapsulating amoxicillin into polyethyleneimine with β-lactamase inhibitor 4-carboxyphenylboronic acid (4-Cpba) decorated HPB nanoparticles (CPA NPs). The antibacterial effect of the CPA NPs on drug-resistant bacteria was observed by *in vitro* colony-forming unit, minimum inhibitory concentration, scanning electron microscopy, and fluorescence tests. The results show that amoxicillin effectively inhibited *Escherichia coli* and *Staphylococcus aureus*-resistant bacteria in the presence of 4-Cpba. The *in vivo* experimental results show that the CPA NPs exhibited a synergistic anti-infective effect *in vivo*, which inhibited the inflammatory response and apoptosis induced by the drug-resistant bacterial infection, and promoted wound healing in mice. The hematoxylin and eosin staining and blood biochemical experiments revealed that the acute toxicity of the material was negligible and it had good biocompatibility. Our results verify our design that CPA NPs can restore the antibacterial activity of amoxicillin.

* Corresponding authors.
E-mail addresses: sunddwj@126.com (D. Sun), doctorwgj66@163.com (G. Wang).
[1] These authors contributed equally to this work.

Peer review under responsibility of King Saud University.

Production and hosting by Elsevier

1. Introduction

Diseases caused by bacterial infections threaten human health and life. Antibiotics play an important role in the treatment of bacterial infections, but the emergence of natural or acquired multi-drug resistant (MDR) bacteria has made some antibiotics ineffective, which seriously threatens public health (Levin and

https://doi.org/10.1016/j.arabjc.2022.103936
1878-5352

B., 2001; Sharkey and O'Neill, 2019; Liu et al., 2021). Bacterial multidrug resistance means that while bacteria are resistant to one antibiotic, they also have cross-resistance to other antibiotics with different structures and different targets, which significantly reduces the drug's chemotherapeutic effect (Liu et al., 2021). MDR bacteria mutate rapidly and have a short reproduction cycle. (Abdallah et al., 2021). The development of new antibiotics has not kept pace with mutation reproduction and MDR bacteria. (Kalan and Wright, 2011). Therefore, identifying new types of antibiotics or antibiotic substitutes has become a problem facing scientific research.

The emergence of bacterial resistance is the product of long-term evolution (Godoy-Gallardo et al., 2021). Resistant mutants are already present before bacteria become susceptible to antibiotics. The abuse of antibiotics has led to huge selection pressure on bacteria. The emergence of drug-resistant bacteria makes commonly used antibiotics ineffective (Crawford et al., 2020; Beha et al., 2021). β-lactamase inhibitors inhibit the activity of β-lactamase, protect the β-lactam ring of antibiotics from hydrolysis, and maintain antibacterial activity. β-lactamase inhibitors are often used in combination with β-lactam antibiotics. There are two types of β-lactam antibiotics, such as those with a β-lactam ring structure and those without a β-lactam ring structure, which are mainly derived from *Streptomyces* bacteria, and chemically synthesized products. The most commonly used β-lactamase inhibitors in clinical practice are sulbactam and clavulanic acid, which are chemically synthesized and are irreversible competitive inhibitors containing the β-lactam ring structure (Impey et al., 2020; Omollo et al., 2021; Parvaiz et al., 2021). Some studies have shown that certain antibiotics can be effective in synergy with bacteria that carry β-lactamases ((Lubna and Khan, 2016; Lubna and Khan, 2017; Maryam and Khan, 2018; Maryam et al., 2019; Islam et al. 2021). Nano drugs are increasingly being used in antibacterial therapy, and nanoparticles (NPs) have a large specific surface area, which improves drug delivery efficiency, enhances therapeutic effects, and reduces toxic side effects. Combination therapy with a drug-resistant inhibitor can overcome the multidrug resistance of bacteria (Pugazhendhi et al., 2020; Srivastava et al., 2021). Douafer et al. reported that combination therapy of amoxicillin and sulbactam achieves good results in clinical treatment and has been widely used (Bush, 2015; Douafer et al., 2020). Sondi et al. reported that the antibacterial activity of NPs was revealed by destroying the cell membranes of bacteria *in vitro* (Sun et al., 2017).

Prussian blue (PB) has been approved by the US Food and Drug Administration for clinical treatment because it has good biocompatibility and is safe (Sondi and Salopek-Sondi, 2004; Xiu et al., 2012; Cai et al., 2019; Busquets and Estelrich, 2020). β-lactamase hydrolyzes the β-lactam ring in the penicillin structure, thereby destroying the structure of the drug and inactivating the penicillin, which is the cause of bacterial resistance (Agnihotri and Jain, 2013; Dacarro et al., 2017; Chen et al., 2020; Guo et al., 2020). Combination therapy of antibiotics and drug-resistant inhibitors has become an effective means for treating drug-resistant bacteria (Beha et al., 2021; Omollo et al., 2021; Parvaiz et al., 2021; Srivastava et al., 2021). 4-Carboxyphenylboronic acid (4-Cpba) is an effective β-lactamase serine protease inhibitor. β-lactamase inhibitors are usually designed as nanomaterials against bacterial resistance (Jiang et al., 2018; Li et al., 2019; Adamczyk-Wozniak et al., 2021; Henry et al., 2021; Huang et al., 2021; Lu et al., 2021). In this study, the β-lactamase inhibitor 4-Cpba-modified Prussian blue-coated amoxicillin NPs were characterized. The results show that the Prussian blue NPs acted as a carrier to deliver the β-lactamase inhibitor and antibiotic and reduced the drug resistance of drug-resistant bacteria by inhibiting the activity of β-lactamase in drug-resistant bacteria. And through *in vitro* and *in vivo* experiments proved that it has antibacterial activity (Scheme 1). These improved NPs can be combined with β-lactamase inhibitor to overcome MDR bacteria.

2. Materials and method

2.1. Bacterial cultures

Escherichia coli ATCC 8739, *Staphylococcus aureus* ATCC 6538, were from in the Biopharmaceutical Laboratory of Anhui Agricultural University, MDR *E. coli* E76227, MDR *S. aureus* ATCC 25213, were from domestic hospitals in China. Resistant forms of *Escherichia coli* $^{(R)}$ and *Staphylococcus aureus* $^{(R)}$ were cultured in LB medium, and the incubator was shaken overnight at 37 °C. On the second day before treatment, the bacterial cells were placed in fresh medium, cultured overnight at 1:100, and incubated in a shaking incubator at 37 °C for 2–3 h until the optical density at 600 nm (OD600) was 0.5.

2.2. Preparation of the PB@amoxicillin NPs

$K_3Fe(CN)_6$ (0.0851 g) and 0.3720 g KCl were dissolved in 50 mL of deionized water as solution 1. Solution 2 was prepared by dissolving 0.0645 g $FeCl_3{\cdot}6H_2O$ and 0.3720 g KCl in 50 mL of deionized water. The pH of solutions 1 and 2 were adjusted to 2 with HCl (12 M). Under vigorous stirring, 25 mL of solution 1 and 3 mL and 55 mg of amoxicillin and polyethyleneimine (PEI) (0.1254 g) were added dropwise to 25 mL of solution 2. The mixture was heated to 60 °C with continuous stirring for 30 min. As the reaction progressed, the mixture gradually turned dark blue. The mixture was centrifuged at 15,000 rpm for about 30 min (Wang et al., 2021a; Wei et al., 2021). The dark blue precipitate was dispersed with 20 mL of DMSO. After repeating this washing three times, the mixture was frozen and stored in a lyophilizer for subsequent experiments (Sondi and Salopek-Sondi, 2004; Busquets and Estelrich, 2020).

2.3. Preparation of the CPA NPs

4-Cpba can be linked to the outside of nanomaterials through an esterification reaction between the amino group on the PB NPs and the carboxyl group on 4-Cpba (Fu et al., 2012; Wei et al., 2021). In short, 600 mg of PB NPs were dissolved in 50 mL of 1% acetic acid solution. 4-Cpba (225 mg) and 230.2 mg of N-hydroxysuccinimide (NHS) were dissolved in 50 mL of methanol and stirred at room temperature for 30 min. 1-Ethyl-(3-dimethylaminopropyl) carbodiimide hydrochloride (383.4 mg; EDC·HCl) was added to the 4-Cpba/NHS mixture and stirred. Then, the 4-Cpba/NHS/EDC·HCl mixture was added to the PB NPs solution (methanol: water was 1:1), stirred at 25 °C for 24 h, and the final product was centrifuged (4 °C, 12,000 rpm, 8 min). The pellet was washed and freeze-dried.

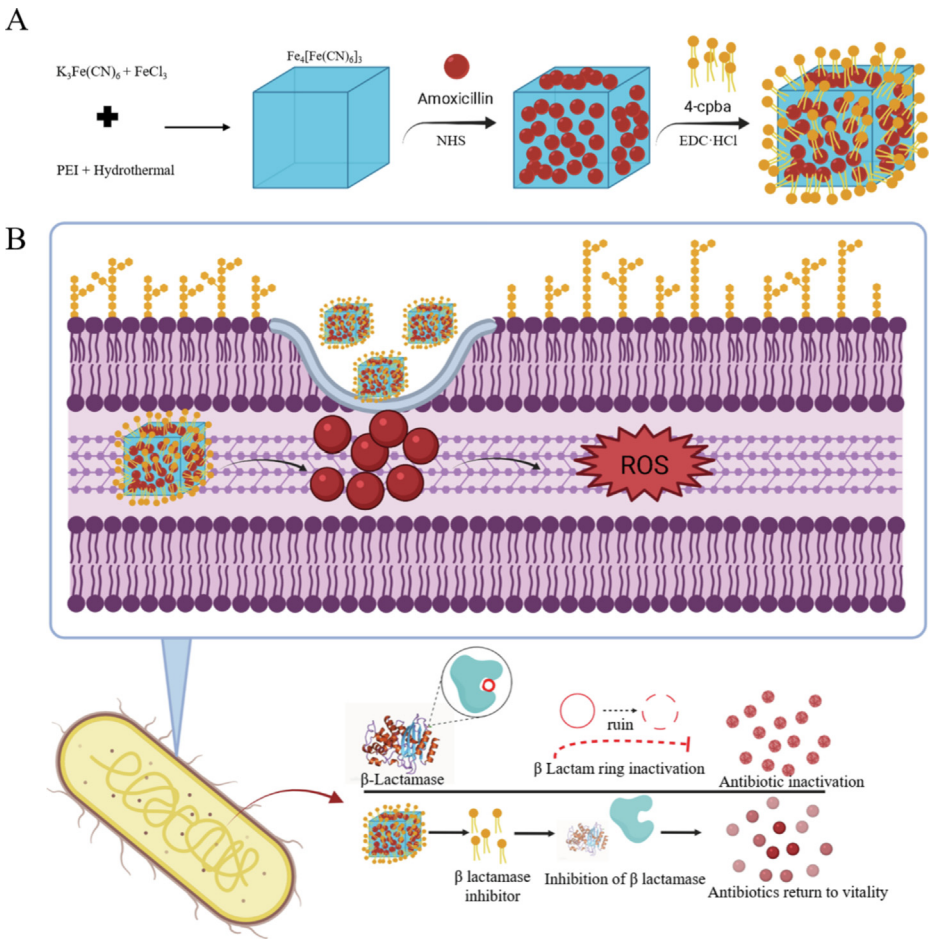

Scheme 1 (A) Synthesis route and research flow chart of CPA NPs and (B) possible antibacterial mechanism.

2.4. Antibacterial activity tests

Colony-forming unit (CFU) counts (Yao et al., 2007; Wang et al., 2016) were used to analyze the number of live bacterial cells in these cultures. Briefly, the log phase bacterial suspensions were co-incubated with 20 μg/mL amoxicillin/NPs in PBS for 24 h in a 37 °C shaker (200 r/min). After incubation, the bacterial suspension was spread evenly on LB solid medium and the total number of colonies was counted manually to evaluate the *in vitro* antibacterial activity. The micro broth dilution method (Zhang et al., 2019) was used to determine the minimum inhibitory concentrations (MIC) of the different solutions (PB NPs, CPA NPs, PB@amoxicillin, amoxicillin, and kanamycin solutions). *S. aureus* $^{(R)}$ and *E. coli* $^{(R)}$ cells grown to the logarithmic phase were cultured on agar plates with different solutions and incubated at 37 °C for 12 h. The MIC value was the lowest drug concentration that inhibited the bacteria. All of the experimental groups contained the same number of bacteria, and all experiments were repeated three times to obtain an average result.

2.5. AO/EB fluorescence experiment

Bacteria (1.5 mL OD600 = 0.5) in the logarithmic growth phase were centrifuged for 5 min and washed several times with PBS (0.01 mol/L) (Yao et al., 2007). The supernatant was discarded and the remaining bacteria were resuspended in 1.5 mL of PBS. The bacteria were treated with 100 μL of 20 μg/mL amoxicillin, PB@amoxicillin, and the CPA NPs. A 100 μL aliquot of fluorescent dye was added and stained for 15 min in the dark. The fluorescent dye was prepared by mixing 10 mg Acridine Orange (AO) and 10 mg ethidium bromide (EB) in 10 mL of PBS. After washing three times with PBS, the bacteria were imaged with a fluorescence microscope. A test without the amoxicillin treatment was used as a control.

2.6. Cell membrane permeability test

We used a reported method to prepare the samples for the membrane permeability analysis (Wang et al., 2016). The dye solution (3 μM propidium iodide, 4 μM diSC3-5) was diluted with culture media, such as HBSS or PBS, to prepare 1–5 mM working solutions. The cells were suspended in the dye working solution at a density of 1×10^6/mL, incubated at 37 °C for 20 min, the labeled suspension tube was centrifuged at 1,000–1,500 rpm for 5 min, and was washed twice. A fluorescence microscope (excitation and emission of 660 nm and 675 nm, respectively) was used for the observations.

The β-galactosidase assay test was reported by Koepse and Russell (Lu et al., 2021). o-Nitrobenzene-b-d-galactoside (50 μL; ONPG) was added to 1 mL of the logarithmic phase *E. coli* $^{(R)}$ (OD600 of 0.5) suspension. Then, the PB NPs were added to this solution. An ultraviolet spectrophotometer was used to measure the absorbance at OD420 nm to evaluate o-

nitrophenol (ONP). A suspension without PB NPs was used as a control.

2.7. Measurement of β-lactamase activity

The nitrocefin color reaction was used to determine bacterial β-lactamase activity (Wang et al., 2021b). The bacterial suspension was incubated with 15 μg/mL amoxicillin or 20 μg/mL CPA NPs at 37 °C for 24 h. Freeze-thawed and killed bacteria were centrifuged at 12,000 rpm at 4℃ for 30 min. The crude bacterial extract was incubated with 0.1 mM nitrocefin, and absorbance was measured by a UV spectrophotometer at 500 nm. The maximum absorption of nitrocefin was recorded, and the color change reflected the β-lactamase activity (Zhao et al., 2013).

2.8. Scanning electron microscopy (SEM) and transmission electron microscopy (TEM)

The bacterial solution was treated with 20 μg/mL amoxicillin or NPs for 24 h and then fixed with 5% glutaraldehyde, dehydrated through an ethanol gradient, and observed by SEM.

The log phase bacterial suspension was treated with 20 μg/mL amoxicillin or NPs at 37 °C for 24 h, and TEM ultrathin sections were prepared according to a previous report (Mushtaq et al., 2010). In short, the treated bacteria were fixed with 5% glutaraldehyde and 1% osmic acid for 1 h. Then, they were dehydrated through a gradient alcohol series, embedded in resin, sliced, and stained with 1% lead citrate solution and 1% uranyl acetate solution for 10 min. Finally, TEM was performed to observe the ultrathin structure of the bacteria.

2.9. Reactive oxygen species (ROS) testing

2′,7′-Dichlorofluorescein diacetic acid (DCFH-DA) was diluted with culture medium to prepare a final concentration of 10 μM. The cells were collected and suspended in the diluted DCFH-DA at a cell concentration of $10^6 \times 10^7$/mL and incubated at 37 °C for 20 min. The suspension was agitated every 3–5 min to allow the probe and cells to make full contact. The cells were washed three times in culture medium to fully remove the DCFH-DA that had not entered the cells. ROS UP was added only to the positive control wells as a positive control. The cells were observed under a fluorescence microscope (excitation and emission were 488 nm and 525 nm, respectively).

2.10. In vivo antibacterial activity

The anti-inflammatory effects of different NPs were tested *in vivo* using a mouse wound healing model. Kunming mice (male, 8-weeks-old, and 30 g) were purchased from Jiangsu Ailingfei Biotechnology Co., Ltd. (Jiangsu, China). After normal feeding for 1 week, 1% pentobarbital was injected into the abdominal cavity for anesthesia, the hair on the chest was shaved, alcohol (75%) was used to disinfect the chest, and a 2 cm round skin wound was cut. The *E. coli* $^{(R)}$ and *S. aureus*$^{(R)}$ suspensions containing 1×10^8 CFU PBS were placed on the left and right wounds, respectively. The wounds were collected 1 day later and cultured in 37 °C LB medium for 12 h to confirm the bacterial infection. Likewise, the samples were extracted 2, 4, 6, and 10 days after surgery and then cultured for detection of antibacterial activity. The drug was injected into the tail vein three times per day to investigate the effect of the drug on wound healing. After the experiment, the dissected mice and wound tissues were collected for hematoxylin-eosin staining (H&E) staining and immunohistochemical analysis.

2.11. Biodistribution of the bacteria and histological analysis

Kunming mice (male, 8-weeks-old 30 g) were used to establish the mouse bacteremia model. After normal feeding for 1 week, a bacterial suspension (1×10^8 CFU) was injected through the tail vein, and a day later, 20 μg/mL CPA NPs (once/day) were injected through the tail vein three times on 3 successive days. The mice were sacrificed on day 5, and blood, heart, liver, spleen, lung, and kidney were collected. The H&E staining and histological analyses were performed on the organs. All mice were raised according to the feeding methods described in the "Guide to Care and Use of Laboratory Animals". The animal experiments were carried out following the protocol approved by the Experimental Animal Center of Anhui Agricultural University (license number: SYXK 2020–007).

2.12. In vivo toxicity analysis

The biological toxicity of PB@amoxicillin and CPA NPs to vital organs (heart, liver, spleen, lung, and kidney) was observed. The experiment was divided into three groups: intravenous injection of PBS (100 μL); intravenous injection of PB@amoxicillin; and intravenous injection of CPA NPs. Injection once a day. The three groups of mice were sacrificed after 30 days and the organs described above were collected from all groups of mice for histopathological analysis. Inductively coupled plasma-atomic emission spectrometry (ICP-AES) was used to determine the content of CPA NPs in the organs, and to quantitatively determine the amount of drug accumulating in each tissue. Hemolytic activity was evaluated in fresh human blood (2.5 mL). The blood was centrifuged at 800 rpm for 10 min, and the supernatant was washed three times with PBS. Then, it was diluted with 50 mL of 5% red blood cell stock solution, mixed with 5 mL of sample solution (10–120 mg/mL) of different concentrations, and incubated at 37 °C for 1 h. Finally, the microplate was centrifuged, and the supernatant (25 μL aliquot) was transferred to a new 96-well plate and further diluted with 50 μL of PBS. Hemolytic activity was measured with a multifunctional microplate reader at OD_{405} nm (Ding et al., 2020).

3. Results and discussion

3.1. Characterization

PB@amoxicillin was about 100 nm on the composite TEM image (Fig. 1A), and the final average diameter of the CPA NPs was 150 nm. Amoxicillin was contained within the PB NPs and 4-Cpba was visible on the surface, with a thickness of about 5 nm (Fig. 1B). The SEM and TEM results showed that the morphology and size of the CPA NPs were consistent.

(Fig. 1C). The dynamic light scattering results confirmed the consistency in the diameter (Fig. 1D). The elemental composition of the CPA NPs was further analyzed by energy dispersive X-ray analysis (Fig. 1E). The results showed that Fe (6.3%) and B (5.9%) in the CPA NPs had stronger signals, which came from the PB NPs and 4-Cpba, respectively. The presence of the N element (9.2%) indicates that the NPs contained a large amount of amoxicillin. The zeta potential of the PB NPs was −11.2 mV (Fig. 1F), and the zeta potential of PB@amoxicillin was 14.9 mV. The changes in the zeta potential were caused by exposure to the surface of the PB@amoxicillin amino groups. The zeta potential of the CPA NPs was −8.3 mV. The zeta potential became negative when the 4-Cpba carboxyl group was exposed. This change in electric potential proves that every step of the modification was successful.

The interaction between PB and PEI was confirmed by infrared spectroscopy. As shown in Fig. 2B, the vibration absorption at 3,403 cm^{-1} was attributed to hydroxyl groups, and the peak at 2,165 cm^{-1} was the vibration absorption of the cyano group in the PB. The absorption bands of the CPA NPs at 770 cm^{-1} and 1,550 cm^{-1} were the characteristic absorption peaks of boric acid and the benzene ring, respectively. These characteristic peaks were reflected on the CPA NPs, indicating that the 4-Cpba-modified PB NPs successfully encapsulated the amoxicillin. The UV–visible spectrum showed that the PB NPs and amoxicillin had characteristic peaks at 300 nm and 240 nm, respectively, and the CPA NP results were similar. PB NPs and CPA NPs have a characteristic UV absorption peak at 750 nm, which is a unique UV absorption peak of PB NPs, while CPA NPs also have similar absorption peaks. Compared with the absorption peaks of PB NPs, it has a red shift. This may be due to PB NPs are modified with 4-Cpba. (Fig. 2A). We investigated the aggregation and sedimentation properties of the CPA NPs to show their thermodynamic and kinetic stability. The light transmittance change in the NPs was < 5% (Fig. 2C), so dynamic stability was high, and there was almost no particle sedimentation. Due to the high thermodynamic stability of the NPs, size did not change significantly within 72 h (Fig. 2D). Good stability is conducive to biological applications of CPA NPs. The amoxicillin release profile of the CPA NPs complexes prepared in PBS buffer at 37 °C is shown in Fig. 2E. The initial release rate of amoxicillin was relatively high, reaching equilibrium at 12 h, and 82% of the amoxicillin was released from the NPs.

3.2. Testing the antibacterial activity of the CPA NPs

The CPA NPs (20 μg/mL) were screened against *S. aureus, E. coli, S. aureus* $^{(R)}$, and *E. coli* $^{(R)}$ using the CFU method. In fact, our CFU test method is to disperse the logarithmically cultured bacterial suspension in co-incubation with different concentrations of material dispersed in PBS for 12 h, and after incubation, the bacterial solution is evenly spread on LB plates and the number of colonies grown is counted to get the survival rate. The CPA NPs had different antibacterial activities against the two species of bacteria (Fig. 3C). The CPA NPs showed higher antibacterial activity than the original amoxicillin and PB@amoxicillin. The survival rates of *S. aureus* $^{(R)}$ and *E. coli* $^{(R)}$ in response to the CPA NPs were 11.3% and 12.4%, respectively. We used the CFU method to count the bacterial cells on LB-agar powder plates. The photographs of the bacterial colonies (S. aureus $^{(R)}$ and *E. coli* $^{(R)}$) that formed on the LB-agar plates were the blank, amoxicillin (20 μg/mL), PB@amoxicillin (20 μg/mL), and CPA NPs (20 μg/mL) groups. The antibacterial activity of the CPA

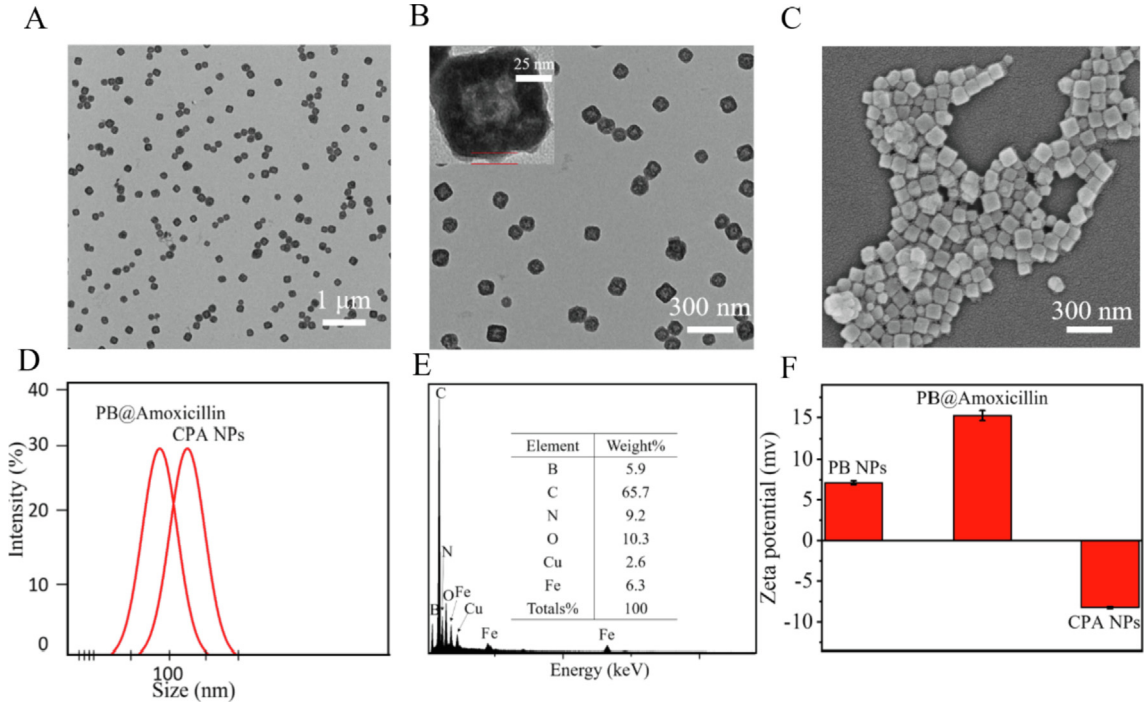

Fig. 1 Morphological characterization of NPs. (A) PB@Amoxicillin TEM images. (B) CPA NPs TEM images. The red part was the 4-Cpba modified layer. (C) SEM images of CPA NPs. (D) Diameters of PB@Amoxicillin, CPA NPs determined at least thrice via DLS. (E) EDX analysis of CPA NPs. (F) Zeta-potentials of PB NPs, PB@Amoxicillin and CPA NPs.

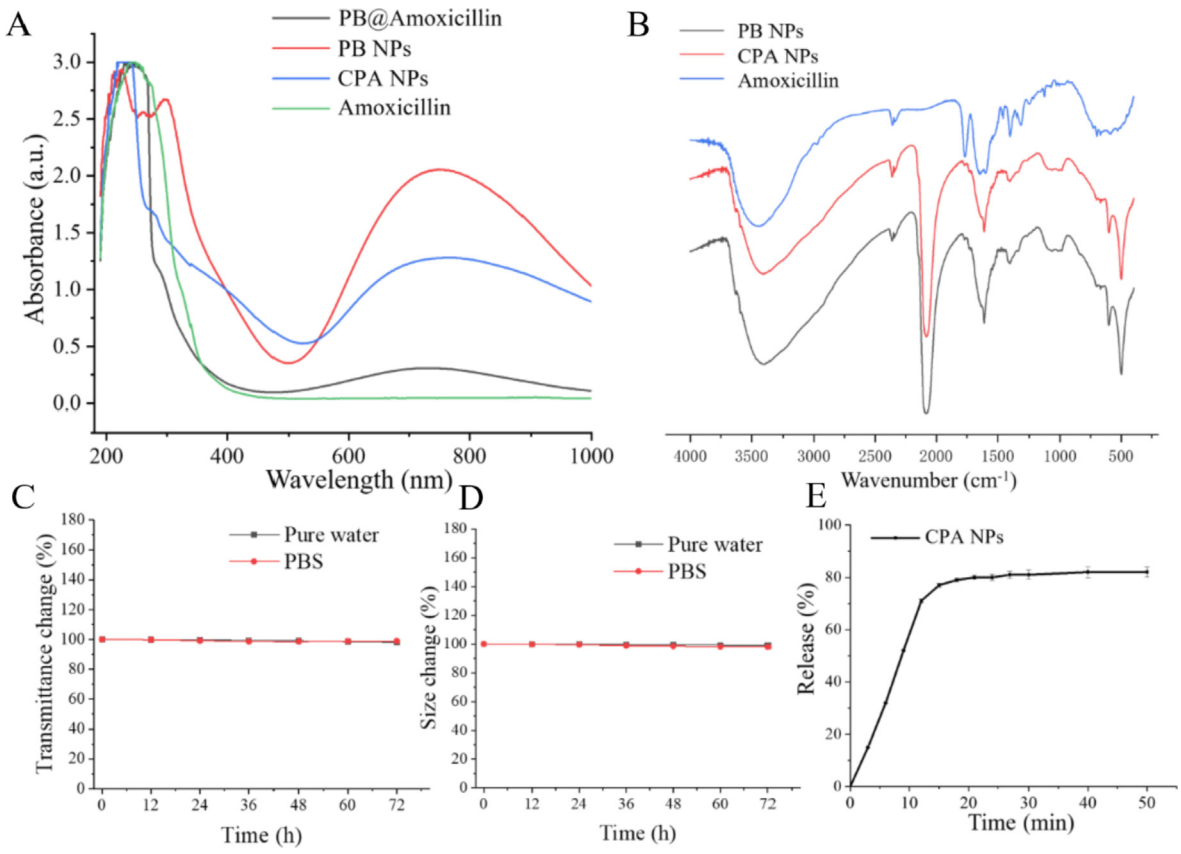

Fig. 2 (A) UV–vis absorption spectra of Amoxicillin, PB NPs, PB@Amoxicillin and CPA NPs. (B) FT-IR spectra of PB NPs, PB@Amoxicillin and CPA NPs. (C) Kinetic stability indicating particle sedimentation; (D) Thermodynamic stability indicating particles aggregation. (E) Amoxicillin release profile of CPA NPs complex prepared in PBS buffer at 37 °C.

NPs was compared with the blank, amoxicillin, and PB@amoxicillin groups. Water was used in the blank group. The CFUs were adjusted. The viability of the bacterial cells was evaluated. The amoxicillin CFU values of *E. coli* $^{(R)}$ and *S. aureus* $^{(R)}$ were 8.5×10^7 CFU/mL and 7.1×10^7 CFU/mL, respectively. Furthermore, the CFU values of PB@amoxicillin of *E. coli* $^{(R)}$ and *S. aureus* $^{(R)}$ were 1.5×10^7 CFU/mL and 1.3×10^7 CFU/mL, respectively. The CPA NPs had the best antibacterial activity, with CFU values (CFU/mL) of 2.4×10^6 for *E. coli* $^{(R)}$ and 1.6×10^6 for *S. aureus* $^{(R)}$. As shown in Fig. 3A, the survival rate of the CPA NPs was much lower than the other three groups. The CPA NPs had better antibacterial activity than the unprocessed amoxicillin and PB@amoxicillin. As shown in Table 1, the MIC of the *S. aureus* $^{(R)}$ CPA NPs was 3.9 μg/mL, while that of *E. coli* $^{(R)}$ was 3.1 μg/mL. Moreover, the MIC of the CPA NPs against *S. aureus* $^{(R)}$ and *E. coli* $^{(R)}$ were lower than those of amoxicillin and PB@amoxicillin. The MIC of the PB NPs for *S. aureus* $^{(R)}$ was 11.2 μg/mL, and the MIC of the PB NPs for *E. coli* $^{(R)}$ was 7.9 μg/mL. The antibacterial activity of the CPA NPs was dominant. The results of *in vitro* experiments showed that the CPA NPs could be used as a new type of NPs for antibacterial testing.

3.3. Fluorescence assay to assess antibacterial activity

LIVE/DEAD staining of *E. coli* $^{(R)}$ and *S. aureus* $^{(R)}$ was carried out using AO and EB fluorescent dyes to determine bacterial viability. In this experiment, the bacterial cells were either green or red under the fluorescence microscope. Green fluorescence indicated live cells and red fluorescence indicated dead cells, and their cell membranes were intact or damaged, respectively. After the cells were treated with different concentrations of the CPA NPs (10 and 20 μg/mL), living cells (red fluorescence) were observed in the blank group (Fig. 4). The number of dead cells was concentration-dependent. The CPA NPs exhibited a stronger inhibitory effect against drug-resistant *S. aureus* $^{(R)}$ and *E. coli* $^{(R)}$ than against amoxicillin and PB@amoxicillin, as shown in Fig. 4(A) and (B). Thus, the results show that the antibacterial activity of amoxicillin was further improved under the action of 4-Cpba and by being wrapped in the PB NPs. The *in vitro* experiments show that our synthesized CPA NPs have a strong antibacterial effect.

3.4. The antibacterial mechanism action of the CPA NPs

As PB NPs can produce ROS, we tested the production of ROS in *E. coli* $^{(R)}$ and *S. aureus* $^{(R)}$ treated with PB NPs. We tested whether oxidative damage is the cause of bacterial death, and whether antibiotics kill bacteria by inducing ROS production. By measuring the total ROS concentration of DCFH-DA, hydroxyl radicals (a type of ROS), and hydroxyphenylfluorescein (HPF), the results showed that the CPA NPs significantly increased ROS production by *S. aureus* $^{(R)}$ and *E. coli* $^{(R)}$ (Fig. 5). As shown in Fig. 5A, the level of intracellular ROS depended on the concentration of CPA NPs. The

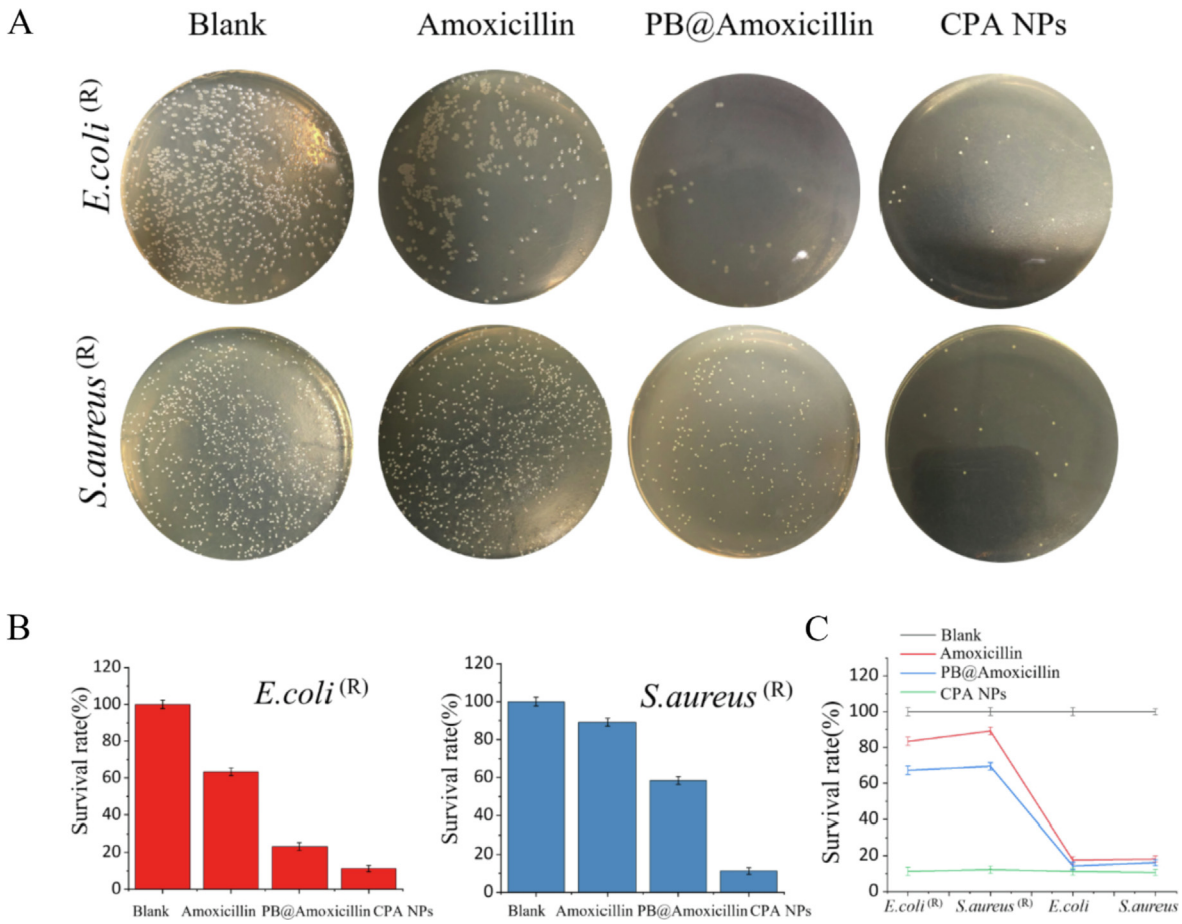

Fig. 3 Testing antibacterial activity of *in vitro*. (A) Photos of bacterial colonies. (*E. coli* $^{(R)}$ and *S. aureus* $^{(R)}$) (B) survival rates of *E. coli* $^{(R)}$ and *S. aureus* $^{(R)}$. (C) Results for *E. coli* $^{(R)}$, *S. aureus* $^{(R)}$, *E. coli*, and *S.aureus* by CFU method, survival rates of bacteria, blank, Amoxicillin (20 μg/mL), PB@Amoxicillin (20 μg/mL), and CPA NPs (20 μg/mL) groups. Each value represents the mean standard deviation (n = 3).

antimicrobial activity of the CPA NPs may be related to the production of ROS by the bacteria. When bacteria was treated with amoxicillin and incubated for 60 min, the ROS levels did not increase, This may be due to β-lactamase inhibiting the activity of amoxicillin, while the ROS levels of *E. coli* $^{(R)}$ treated with CPA NPs increased significantly (Fig. 5B). These results suggest that one of the mechanisms by which CPA NPs kill bacteria is the production of ROS. Bacterial cell membranes are damaged by nanocomposites. When CPA NPs enter cells by destroying the cell membrane of the bacteria, it induces high levels of ROS production, This process causes oxidative damage, affects bacterial activities, and kills bacteria, leading to high antibacterial activity.

We quantified the bacterial membranes damaged by NPs with a fluorescent dye. PI passes through the damaged cell membrane and enters the interior to fluoresce with nucleic acids. The cyanine dye diSC3-5(3,3′-dipropylthiadicarbocya nine iodide) binds to the plasma membrane and fluorescence quenching occurs. When the plasma membrane is damaged, the dye is released, and the integrity of the bacterial cell membrane and cytoplasm are determined by PI and diSC3-5. The higher the fluorescence intensity, the more serious the damage. Compared with the negative control, amoxicillin caused only a small increase in the fluorescence of the dye, which may be related to the hydrolysis of the lactam ring in amoxicillin by the β-lactamase of drug-resistant bacteria. When the cells were treated with PB@amoxicillin and CPA NPs, the cell membrane permeability of *E. coli* $^{(R)}$ and *S. aureus* $^{(R)}$ increased significantly. PB@amoxicillin and CPA NPs also increased cytoplasmic membrane permeability of *E. coli* $^{(R)}$ and *S. aureus* $^{(R)}$. Amoxicillin had only a weak effect on cell wall permeability of *S. aureus* $^{(R)}$. These results show that the CPA NPs caused extensive damage to the bacterial cell and plasma membranes (Fig. 6). The CPA NPs exhibited extensive antibacterial activity by increasing the permeability of cell walls and plasma membranes.

To further demonstrate destruction of the bacterial membrane, we measured the release of β-galactosidase from *E. coli* $^{(R)}$. β-galactosidase is found in the cytoplasm of *Enterobacteriaceae* (e.g., *E. coli* $^{(R)}$). This enzyme is released into the culture medium when the plasma membrane of a cell is destroyed, which catalyzes the production of O-nitrophenol (ONP) by ONPG. Therefore, ONPG was added to the cultures, and the change in the amount of ONP in the medium was measured by measuring the OD_{420nm} value to determine whether the bacterial cell membrane was destroyed. Fig. 6C shows that as the concentration of the NPs was increased, the release of cytosolic β-galactosidase from the *E. coli* $^{(R)}$ sus-

Table 1 MIC values about *E. coli* $^{(R)}$ and *S. aureus* $^{(R)}$.

Bacteria	PB NPs (μg/mL)	PB@Amoxicillin (μg/mL)	CPA NPs (μg/mL)	Amoxicillin (μg/mL)	Kanamycin (μg/mL)
S. aureus $^{(R)}$	11.2 ± 0.51	7.5 ± 0.15	3.9 ± 0.31	5.3 ± 0.12	0.4 ± 0.04
E. coli $^{(R)}$	7.9 ± 0.21	6.4 ± 0.19	3.1 ± 0.09	6.4 ± 0.21	0.9 ± 0.07

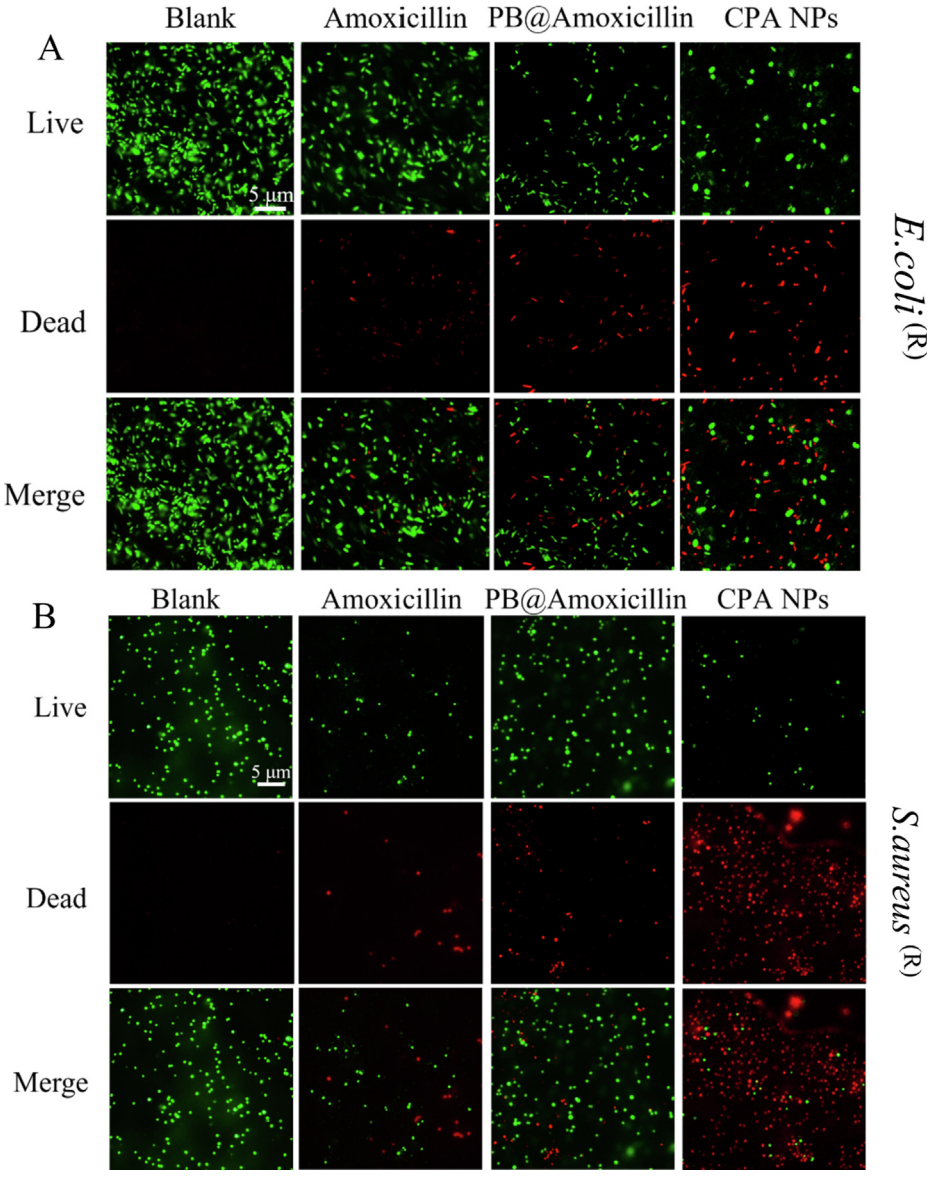

Fig. 4 Fluorescence microscopic images of drug-resistant *E. coli* $^{(R)}$ (A) and *S. aureus* $^{(R)}$ (B) through the LIVE-DEAD stained assay. Cells treated with Amoxicillin (20 μg/mL), PB@Amoxicillin (20 μg/mL), CPA NPs (20 μg/mL) were set as control groups. Cells were treated with CPA NPs (20 μg/mL) for 2 h in incubation. The blank group is bacteria without NPs.

pension increased with time. These results indicate that treatment with CPA NPs damaged the integrity of the membranes, which caused cytoplasmic enzymes to be released into the medium. This result shows that the CPA NPs bind to the surface of the bacterial cell membrane, cause damage, and kill the bacteria.

3.5. CPA NPs inhibit β-lactamase activity

One of the main reasons for bacterial resistance is the overexpression of β-lactamase by bacteria, which decomposes β-lactam antibiotics and promotes drug resistance. Inhibiting the expression or activity of β-lactamase is a new strategy to

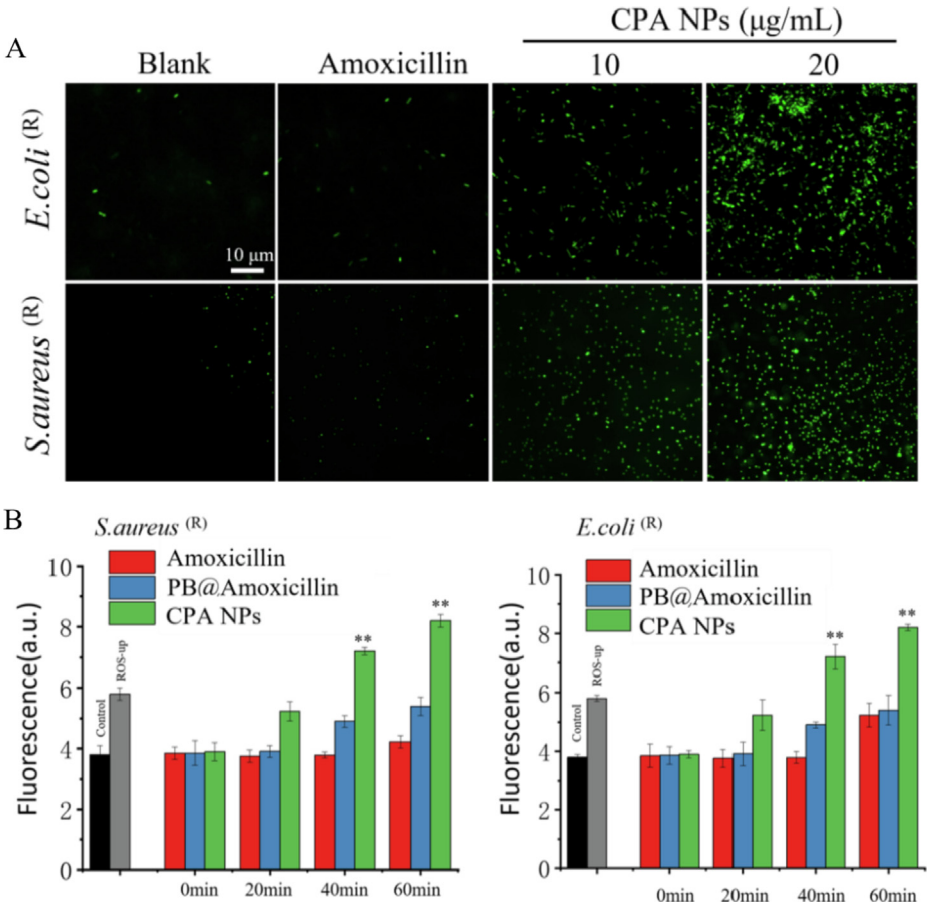

Fig. 5 (A) After incubating for 30 min with 10 mM DCFH-DA in PBS, 10 μg/mL and 20 μg/mL CPA NPs and amoxicillin were used for 60 min at 32℃, and imaging was performed under a fluorescence microscope. The blank group is without NPs. (B) Cellular total ROS probed with 20,70- dichlorofluorescein diacetate (DCFH-DA), use the microplate reader to detect the total ROS of the cells, the positive control is to add the Ros-up in the kit. (*p < 0.05, **p < 0.01 Amoxicillin-treated group vs. no Amoxicillin-treated group) Each value represents the mean standard deviation (n = 3).

reverse antibiotic resistance. β-lactamase hydrolyzes the amide bond of nitrocefin and produces a color reaction. The shift in the maximum absorbance peak from 380 nm (yellow) to 500 nm (red) reflects the change in β-lactamase activity. The maximum absorption peak shifted from 380 nm (yellow) to 500 nm (red) by imaging the color change (Fig. 6D). The color changed from yellow to red, confirming the inhibitory effect of the CPA NPs on β-lactamase activity. Fig. 6E shows that the bacterial extract treated with amoxicillin decomposed nitrocefin. Absorbance at 500 nm increased with time, and decomposition became more rapid and intense as the concentration of amoxicillin was increased. Moreover, the CPA NPs effectively inhibited β-lactamase activity in a time-dependent manner. A quantitative analysis of β-lactamase activity further confirmed this inhibitory effect (Fig. 6D). In summary, CPA NPs effectively inhibited the β-lactamase activity of drug-resistant bacteria.

3.6. Cell integrity studies

The morphological changes in *S. aureus* $^{(R)}$ and *E. coli* $^{(R)}$ treated with CPA NPs were observed by SEM. SEM revealed the damage to the bacterial membranes (Fig. 7). After 12 h of incubation, CPA NPs were added to the *E. coli* $^{(R)}$ and *S. aureus* $^{(R)}$ cultures to maintain the integrity of the membrane structure. The enlarged area (control) shows that the bacterial cells were smooth and had a complete cell membrane. In contrast, cell integrity was compromised in cells treated with the CPA NPs for 12 h compared with untreated cells. The number of *S. aureus* $^{(R)}$ and *E. coli* $^{(R)}$ cells decreased after treatment with the CPA NPs, the cell membranes wrinkled, and intracellular contents were damaged. Damage was still observed on the surface of most cells at a high concentration of CPA NPs (20 μg/mL), while leakage of intracellular contents was observed in most *S. aureus* $^{(R)}$ and *E. coli* $^{(R)}$ cells, as shown in Fig. 7. The form and size of the cells changed significantly. The TEM ultra-thin sections showed that the cytoplasm of healthy *E. coli* $^{(R)}$ and *S. aureus* $^{(R)}$ cells were uniform and complete (Fig. 8A, B). However, *E. coli* $^{(R)}$ and *S. aureus* $^{(R)}$ showed obvious cell lysis, cavitation, and rupture of the membranes after treatment with amoxicillin, PB@amoxicillin, and CPA NPs (Fig. 8A, B). As expected, the CPA NPs treatment created more damage to the morphology of the resistant bacteria, which was concentration-dependent. The results show that the CPA NPs had a significant antibacterial effect on the cells, and that the CPA NPs changed the morphology

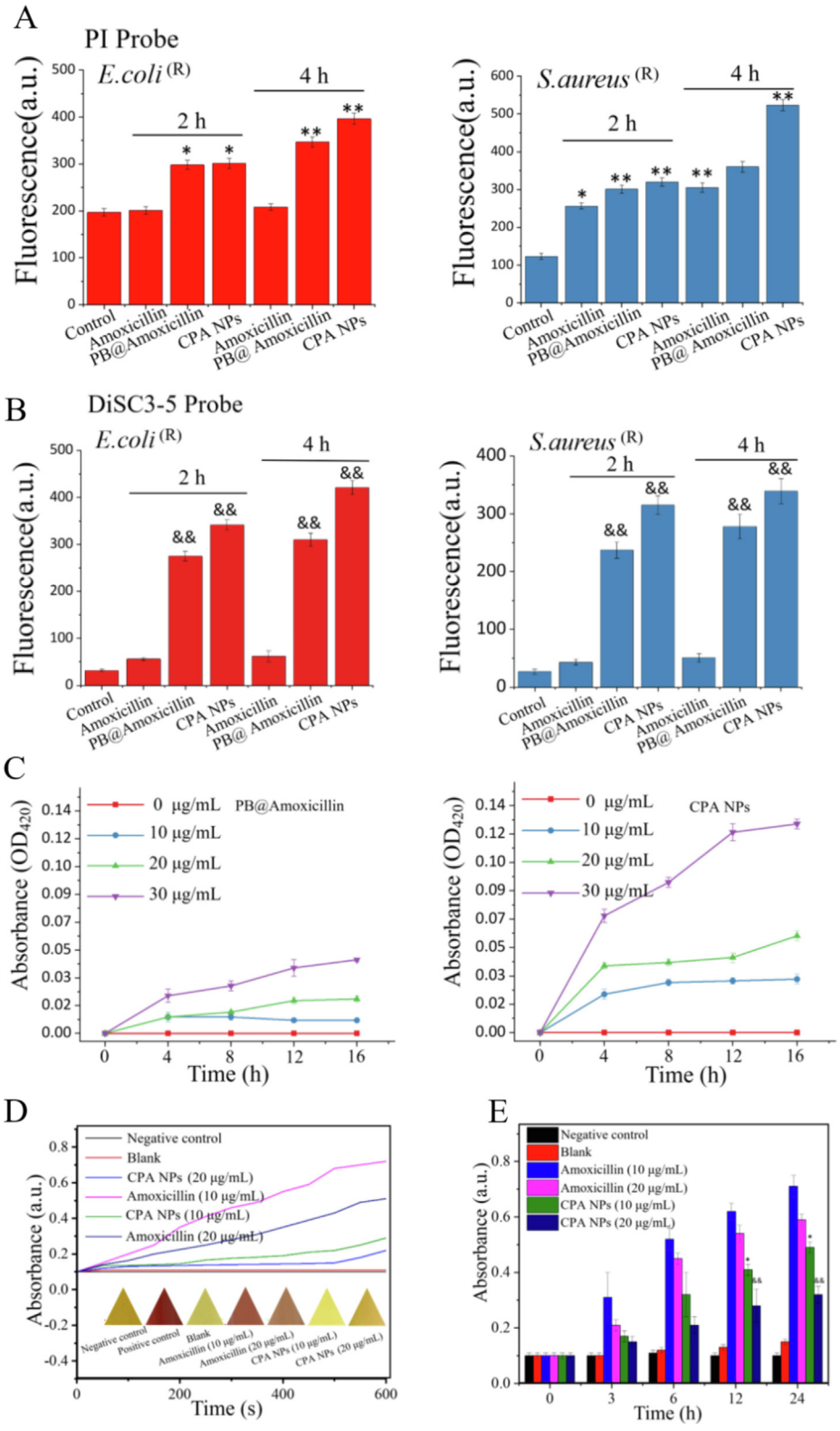

Fig. 6 (A) PI and (B) DiSC3-5 were used to detect the integrity of bacterial cells and cytoplasmic membranes. The test without NPs was used as a control. The increase in fluorescence corresponds to the degree of damage to the total cell membrane. (C) Treat the absorption of ONP with PB@Amoxicillin and CPA NPs different time and concentration with *E. coli* $^{(R)}$. (D) Test the activity of β-lactamase. Detect the absorbance of nitrocefin at 500 nm. Bacterial crude extract with 0.1 mM nitro cephalosporin incubation, the absorbance was measured at 500 nm. The color change of triangle is nitrocefin under white light. (E) Histogram of β-lactamase activity over time. (&p < 0.05, &&p < 0.01 *p < 0.05, CPA NPs treatment group). Each value represents the mean standard deviation (n = 3). Each value represents the mean standard deviation (n = 3).

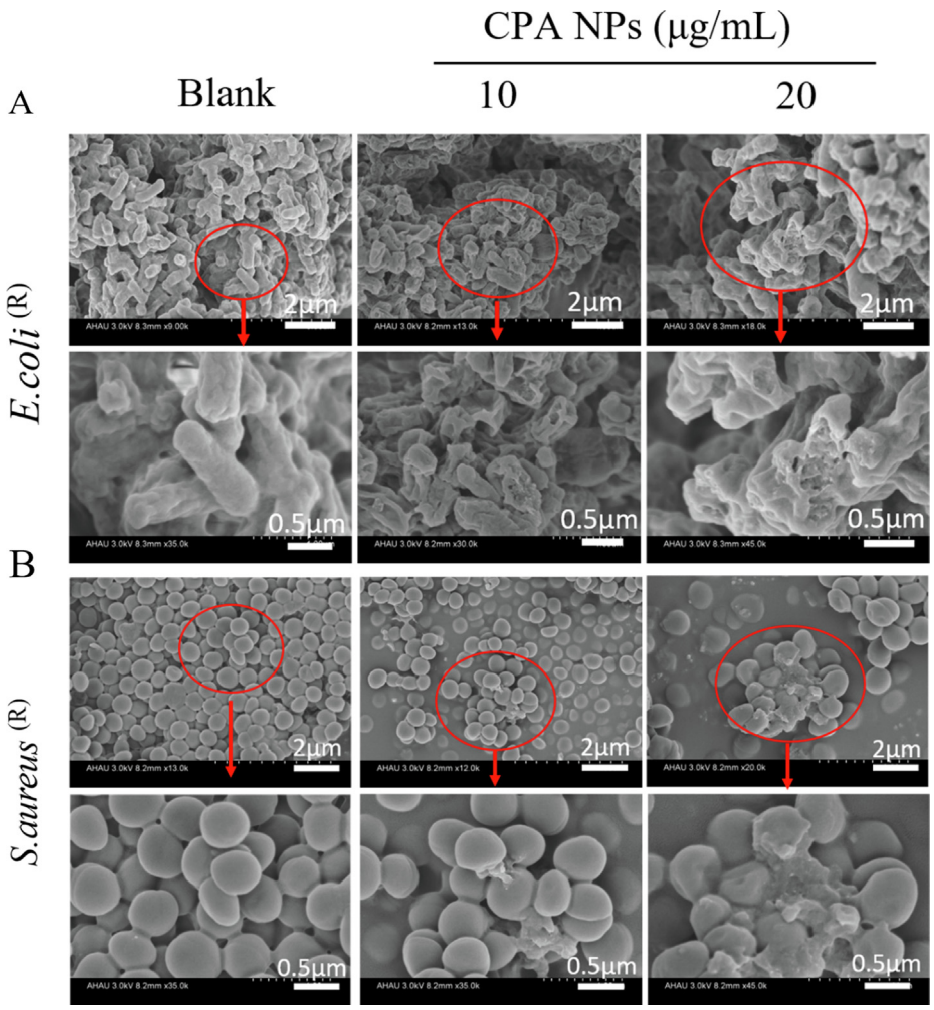

Fig. 7 Morphological changes of *E. coli* $^{(R)}$ (A) and *S. aureus* $^{(R)}$ (B) treated with CPA NPs (10 and 20 μg/mL). The part in the red rectangles is enlarged. The blank group is bacteria without NPs.

of the bacterial cells. This effect may eventually lead to cell death. The morphological change mechanism of *S. aureus* $^{(R)}$ and *E. coli* $^{(R)}$ indicates that the bacterial cell membranes were damaged because the synergistic effect of PB and amoxicillin enhanced antibacterial activity. The NPs loaded with amoxicillin and 4-Cpba penetrated the bacterial cell membrane and cell wall. 4-Cpba ensured that the amoxicillin was not hydrolyzed by β-lactamase, so that it could kill the drug-resistant bacteria. This is the main antibacterial mechanism of the nanocomposites.

3.7. In vivo wound recovery

To compare the therapeutic effects of nanomaterials on drug-resistant bacteria *in vivo*, we further tested their antibacterial activity in mice. Wounds were created and *E. coli* $^{(R)}$ and *S. aureus* $^{(R)}$ were added to the left and right chest wounds, respectively. The conventional β-lactamase inhibitor clavulanic acid is associated with adverse effects when coadministered with amoxicillin, whereas CPA NPs have a good biosafety profile with few toxic side effects. We used clavulanic acid (the most commonly used β-lactamase inhibitors in clinical practice) in combination with amoxicillin, and CPA NPs as the experimental group. Daily intravenous injections of amoxicillin + clavulanic acid (2:1) acid or the CPA NPs and wound healing were recorded and imaged (Fig. 9A). The results showed no significant changes in wound healing after the *E. coli* $^{(R)}$ and *S. aureus* $^{(R)}$ infections in the blank group and the amoxicillin + clavulanic acid treated group, as shown in the wound images (Fig. 9A, C, D). Moreover, The CPA NPs treatment effectively promoted wound healing after the *E. coli* $^{(R)}$ and *S. aureus* $^{(R)}$ infections compared with the blank group and the amoxicillin + clavulanic acid treated group. Fig. 9A is a photograph of wound healing in the mice. The wounds in the CPA NPs treatment group were completely epithelialized on day 10 after surgery, and these tissues were comparable to healthy tissues. In short, the CPA NPs were effective for treating wounds. Wound tissue H&E staining experiments were performed to study the pathological changes in the nanocomposite sites of infection in the muscle tissue. Fig. 9B compares the images produced by differently processed tissues. The degree of wound tissue infection was highest in the untreated group compared with the control group. The degree of inflammation in the amoxicillin + clavulanic acid-treated group was lower than that in the untreated group. In contrast, tissue sections treated with the CPA NPs showed no obvious signs of

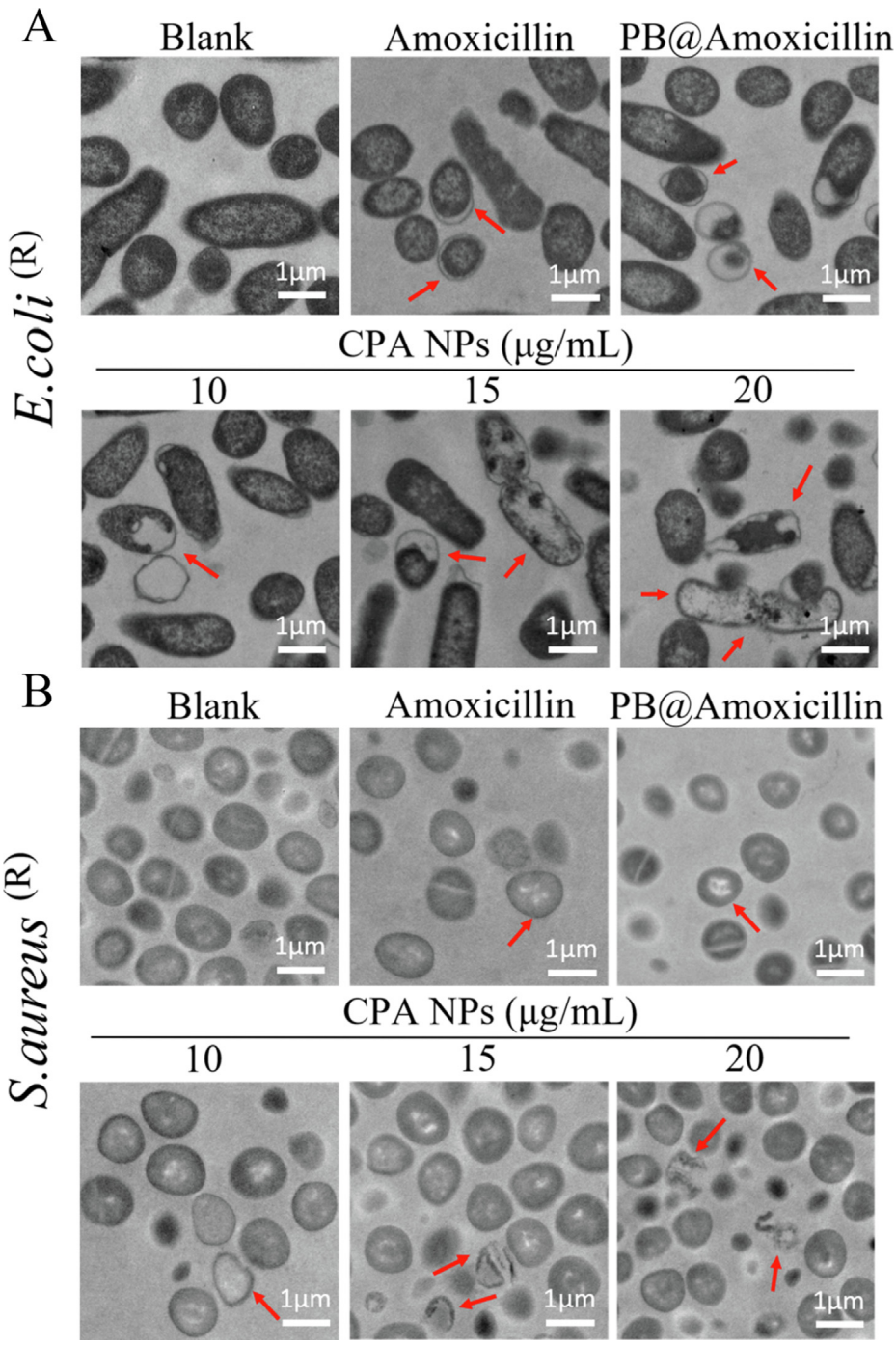

Fig. 8 Morphological changes of *E. coli* $^{(R)}$ (A) and *S. aureus* $^{(R)}$ (B) Treated with Amoxicillin, PB@Amoxicillin and CPA NPs (10,15 and 20 μg/mL) through TEM observation. Assay without NPs is as blank. The red arrow points to the broken part of the bacterial cell membrane.

inflammation, which was very similar to the control group. In addition, epithelial cell growth was observed and granulation tissue formed, suggesting tissue healing. Immunohistochemistry confirmed that the CPA NPs effectively reduced inflammation of the infected tissues. Fig. 9D shows the corresponding wound sizes of the *E. coli* $^{(R)}$ and *S. aureus* $^{(R)}$ infections in the mice. These *in vitro* and *in vivo* experiments show that CPA NPs have potent antibacterial effects that promote wound healing.

3.8. Histopathological inspection of animal organs and tissues

On day 7 after the injection, the abdomen was incised and organs, such as the heart, liver, kidneys, spleen, and lungs were collected. The mouse organs were imaged (Fig. 10). The organs in the blank group were normal. The animal organs inoculated with bacteria showed obvious signs of inflammation or lesions produced by *S. aureus* $^{(R)}$. As shown in Fig. 10A, all organs

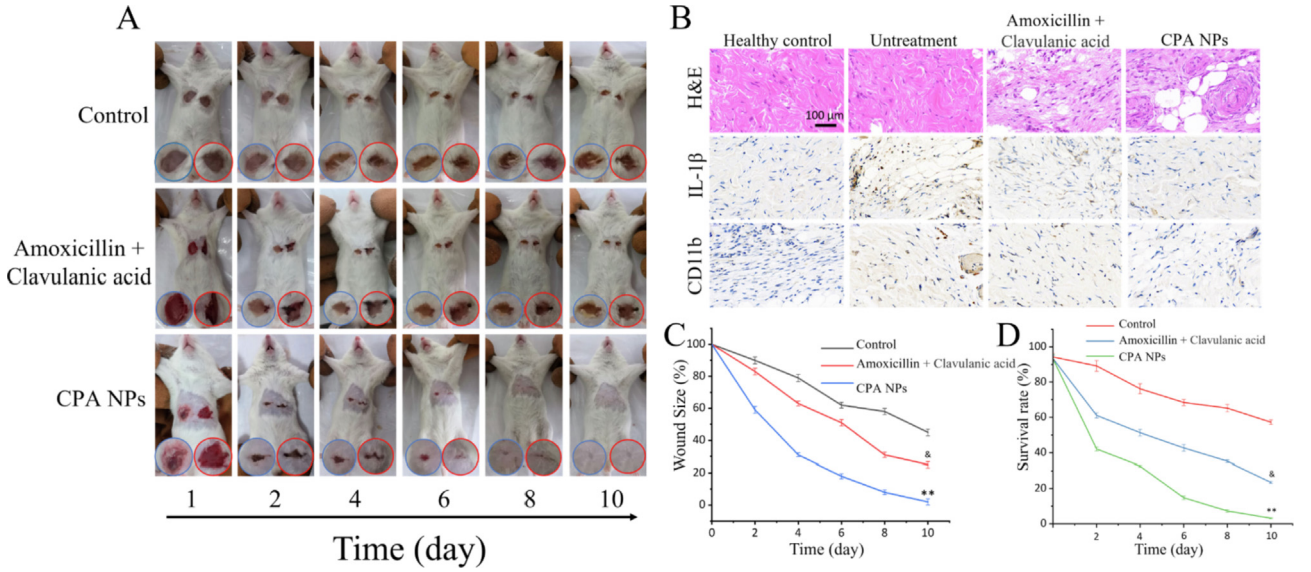

Fig. 9 (A)Representative photos of wounds infected with bacteria treated with Amoxicillin + Clavulanic acid or CPA NPs (and untreated mice used as controls) (B) H&E staining images and immunohistochemical results of the wound tissue sections; (C) Diagram of the change in wound size over time after MDR bacterial infection ($^{\&}p < 0.05$, $^{\&\&}p < 0.01$ Amoxicillin + Clavulanic acid treatment group and control group; $^{*}p < 0.05$, $^{**}p < 0.01$ CPA NPs treatment group and control group); (D) Count statistics of bacterial cultures in tissues of untreated and CPA NPs-treated wounds; Each value represents the mean standard deviation (n = 3).

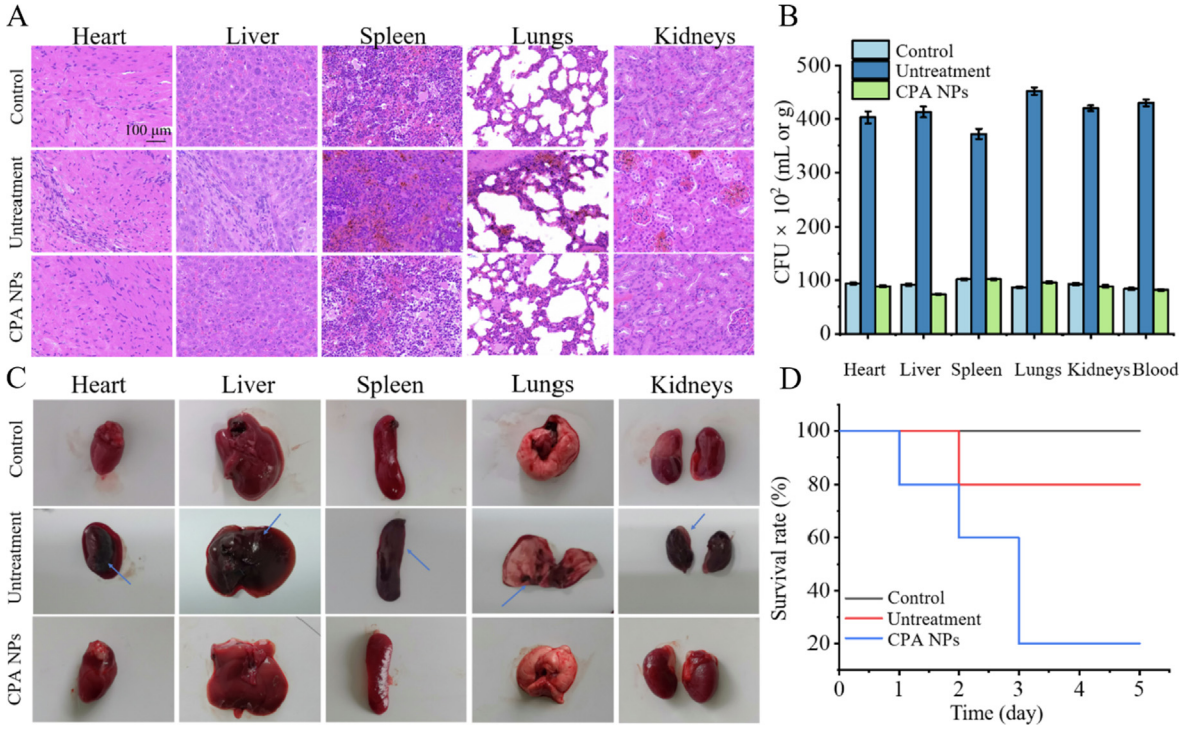

Fig. 10 (A) Histological methods were used to detect the bacteremia model of CPA NPs and the therapeutic effect. The main organs of the mice were examined histologically after 5 days *S. aureus* $^{(R)}$ intravenously. Compared with the blank group, the infected group had inflammatory cells. The concentration of NPs is 20 μg/mL. (B) Bacterial burden in heart, liver, spleen, lungs, kidneys and blood. (C) Representative images of organs treated with saline (control group), *S. aureus* $^{(R)}$ (untreatment group), *S. aureus* $^{(R)}$ + CPA NPs (treatment group) for 5 days. Observe inflammatory symptoms and lesions on imaging. The blue arrow indicates necrosis and abscess. The concentration of NPs is 20 μg/mL. (D) Five-day survival rate of mice infected by *S. aureus* $^{(R)}$ infection.

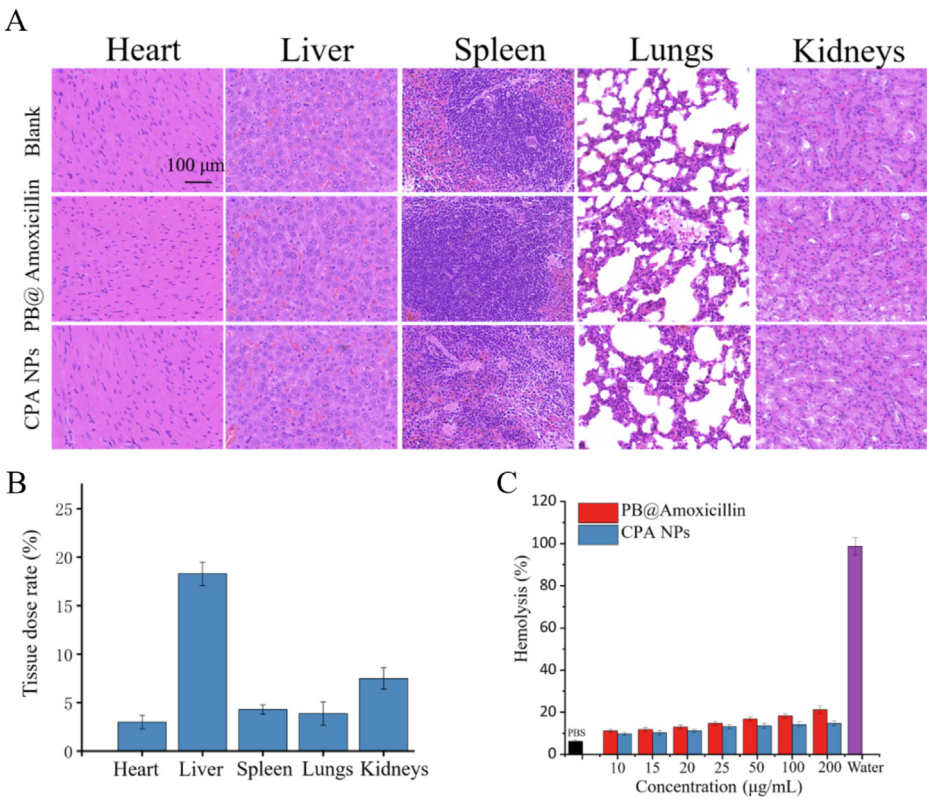

Fig. 11 Toxicity nano composite material evaluation by H&E staining. Mice treated with 1.0 mL PBS were used as the control group, and mice injected with PB@Amoxicillin or CPA NPs were used as the treatment group. (B) Biodistribution of Fe in mice treated with CPA NPs. Fe concentrations are shown in heart, liver, spleen, lung, and kidney of mice. (C) Hemolysis results of unlike concentrations of PB@Amoxicillin and CPA NPs. The concentration of NPs is 20 μg/mL. Each value represents the mean SD (n = 3).

were infected and presented symptoms of inflammation and necrosis. After bacteremia model (infection group) mice CPA NPs (20 μg/mL) treatment, mice were treated organ functions properly. The bacteremia model was successful after comparing the two groups (control group and infected group). The number of bacteria in blood, heart, liver, spleen, lung and kidney was significantly increased after *S. aureus* $^{(R)}$ infection (Fig. 10B). The results of the three groups show that the CPA NPs killed *S. aureus* $^{(R)}$ and cured the bacteremia caused by *S. aureus* $^{(R)}$. In contrast, as shown in Fig. 10A, these data provide visual observations of the inflammation and lesions caused by *S. aureus* $^{(R)}$ in the infected group. No obvious histopathological abnormalities or lesions were detected in the treatment group. Some inflammatory cells were observed in the organs. These results indicate that CPA NPs may be a way to treat bacteremia. After the tail vein injection of *S. aureus* $^{(R)}$ suspension, the survival rate of mice was only 20% (Fig. 10D). To further study the *in vivo* biocompatibility of CPA NPs, we used H&E staining for a histopathological analysis of the organs of the mice. The heart, liver, spleen, lungs, and kidneys of the mice were used to study the tissue damage, inflammation, and the pathology caused by the CPA NPs.

3.9. Biosafety evaluation

The above experiments showed that the CPA NPs have strong antibacterial activity *in vivo* and *in vitro*. The CPA NPs are nanomaterials with antibacterial effects. An investigation of biological toxicity is necessary for a nanocomposite material. We analyzed the histological changes in mice that were continuously injected with PB@amoxicillin and CPA NPs for 30 days to define whether the nano-composite and drugs affected the mice. The H&E staining results of the organs of the mice had normal physiological characteristics compared with the control group, and there were no problems, such as cell apoptosis or tissue damage (Fig. 11A). This result indicates that PB@amoxicillin and CPA NPs were biocompatible with the mice. The remnant amount of Fe in the mice organs was measured (Fig. 11B) by ICP-AES after 48 h. The remaining iron was limited except in the liver and kidneys. This result shows that NPs can be efficiently eliminated from the mice without causing damage. We also tested the hemolytic activity of the CPA NPs. The results are shown in Fig. 11C. The hemolytic rate increased with the increase in the NPs concentration. However, the increase was small, and the samples did not reveal significant hemolysis behavior, indicating very low cytotoxicity to the cells. The results of the toxicity test showed that the CPA NPs exhibited few side effects and low toxicity *in vivo* and *in vitro*, and have potential clinical value.

4. Conclusions

In this study, PB nanoparticles were synthesized for the coordinated delivery of amoxicillin and a β-lactamase inhibitor.The conventional β-lactamase inhibitor clavulanic acid is associated with adverse effects when coadministered with amoxi-

cillin, whereas CPA NPs have a great biosafety profile with few toxic side effects. The β-lactamase inhibitor 4-Cpba effectively inhibited β-lactamase activity and synergistically enhanced the *in vitro* antibacterial activity induced by amoxicillin. The antibacterial effect of the CPA NPs on *E. coli* $^{(R)}$ and *S. aureus* $^{(R)}$ was observed by *in vitro* CFU, MIC, SEM, and fluorescence tests. Because of the presence of this resistance mechanism, CPA NPs can also prevent bacteria from developing drug-resistant mutations.The results show that the CPA NPs exhibited cell uptake, destroyed cell walls, and inhibited bacterial reproduction. We speculate that the reason for these results may be that the 4-Cpba bound firmly to β-lactamase to irreversibly inactivate the enzyme, protecting the enzyme-intolerant amoxicillin from being destroyed, thereby allowing the latter to enter the site of action. The results show that amoxicillin and the β-lactamase inhibitor mediated by nano-PB composites and β-lactamase inhibitors also performed *in vivo*. They had a synergistic anti-infection effect, inhibited the cell apoptosis induced by *E. coli* $^{(R)}$ and *S. aureus* $^{(R)}$ infection, and promoted wound healing. The H&E tissue staining showed that the CPA NPs significantly inhibited the bacteremia caused by *S. aureus* $^{(R)}$ infection *in vivo*, but they were not toxic to the organs of mice, which demonstrates good biocompatibility *in vivo*. Our results validate that a PB nanocomposite co-delivering amoxicillin and a β-lactamase inhibitor may be an efficient way to overcome drug-resistant bacteria and achieve synergistic antibacterial effects.

Funding

This work was supported by 2021 Fuyang City Science and Technology Major Special Project (FK20208005), Excellent young talents support program in Colleges and Universities of Anhui Province (gxyqZD2020006), and Scientific Research Project of Anhui Education Department (KJ2019A0182), the Key R&D Projects in Anhui Province (202104f06020028), Major Science and Technology Project of Anhui Province (17030701023), Shandong Province Medical and Health Technology Development Plan (2019WS210).

References

Abdallah, K., Tharwat, A., and Gharieb, R. (2021). High efficacy of a characterized lytic bacteriophage in combination with thyme essential oil against multidrug-resistant Staphylococcus aureus in chicken products. Iranian J. Veterinary Res. 22(1), 24–32. 10.22099/ijvr.2020.38083.5543.

Adamczyk-Wozniak, A., Gozdalik, J.T., Kaczorowska, E., Durka, K., Wieczorek, D., Zarzeczanska, D., et al, 2021. (Trifluoromethoxy) Phenylboronic Acids: Structures, Properties, and Antibacterial Activity. Molecules 26 (7). https://doi.org/10.3390/molecules26072007.

Agnihotri, J., Jain, N.K., 2013. Biodegradable long circulating cellular carrier for antimalarial drug pyrimethamine. Artif. Cells Nanomed. Biotechnol. 41 (5), 309–314. https://doi.org/10.3109/21691401.2012.743901.

Beha, M.J., Ryu, J.S., Kim, Y.S., and Chung, H.J. (2021). Delivery of antisense oligonucleotides using multi-layer coated gold nanoparticles to methicillin-resistant S. aureus for combinatorial treatment. Mater. Sci. Eng. C-Mater. Biol. Appl. 126. 10.1016/j.msec.2021.112167.

Bush, K., 2015. Investigational Agents for the Treatment of Gram-Negative Bacterial Infections: A Reality Check. ACS Infect. Dis. 1 (11), 509–511. https://doi.org/10.1021/acsinfecdis.5b00100.

Busquets, M.A., Estelrich, J., 2020. Prussian blue nanoparticles: synthesis, surface modification, and biomedical applications. Drug Discovery Today 25 (8), 1431–1443. https://doi.org/10.1016/j.drudis.2020.05.014.

Cai, S., Qian, J., Yang, S., Kuang, L., Hua, D., 2019. Acetylcysteine-decorated Prussian blue nanoparticles for strong photothermal sterilization and focal infection treatment. Colloids and Surfaces B-Biointerfaces 181, 31–38. https://doi.org/10.1016/j.colsurfb.2019.05.007.

Chen, X., Wu, G., Tang, J., Zhou, L., Wei, S., 2020. Ytterbium - Doped Prussian blue: Fabrication, photothermal performance and antibacterial activity. Inorg. Chem. Commun. 114. https://doi.org/10.1016/j.inoche.2020.107821.

Crawford, C.L., Dalecki, A.G., Perez, M.D., Schaaf, K., Wolschendorf, F., Kutsch, O., 2020. A copper-dependent compound restores ampicillin sensitivity in multidrug-resistant Staphylococcus aureus. Sci. Rep. 10 (1). https://doi.org/10.1038/s41598-020-65978-y.

Dacarro, G., Grisoli, P., Borzenkov, M., Milanese, C., Fratini, E., Ferraro, G., et al, 2017. Self-assembled monolayers of Prussian blue nanoparticles with photothermal effect. Supramol. Chem. 29 (11), 823–833. https://doi.org/10.1080/10610278.2017.1372582.

Ding, X., Yin, C., Zhang, W., Sun, Y., Zhang, Z., Yang, E., et al, 2020. Designing Aptamer-Gold Nanoparticle-Loaded pH-Sensitive Liposomes Encapsulate Morin for Treating Cancer. Nanoscale Res. Lett. 15 (1). https://doi.org/10.1186/s11671-020-03297-x.

Douafer, H., Andrieu, V., Phanstiel, O., Brunel, J.M., 2020. Antibiotic Adjuvants: Make Antibiotics Great Again! (vol 62, pg 8665, 2019). J. Med. Chem. 63 (3), 1440. https://doi.org/10.1021/acs.jmedchem.9b02109.

Fu, G., Wei, L., Feng, S., and Yue, X.J.C.C. (2012). Prussian blue nanoparticles operate as a new generation of photothermal ablation agents for cancer therapy. 48(94), 11567–11569.

Godoy-Gallardo, M., Eckhard, U., Delgado, L.M., de Roo Puente, Y. J.D., Hoyos-Nogues, M., Gil, F.J., et al, 2021. Antibacterial approaches in tissue engineering using metal ions and nanoparticles: From mechanisms to applications. Bioact. Mater. 6 (12), 4470–4490. https://doi.org/10.1016/j.bioactmat.2021.04.033.

Guo, R., Chen, Y., Nengzi, L.-C., Meng, L., Song, Q., Gou, J., et al, 2020. In situ preparation of carbon-based Cu-Fe oxide nanoparticles from CuFe Prussian blue analogues for the photo-assisted heterogeneous peroxymonosulfate activation process to remove lomefloxacin. Chem. Eng. J. 398. https://doi.org/10.1016/j.cej.2020.125556.

Henry, P., Halbus, A.F., Athab, Z.H., and Paunov, V.N. (2021). Enhanced Antimould Action of Surface Modified Copper Oxide Nanoparticles with Phenylboronic Acid Surface Functionality. *Biomimetics (Basel, Switzerland)* 6(1). 10.3390/biomimetics6010019.

Huang, Y., He, Y., Xia, X., Quan, H., Yu, J., 2021. Phenylboronic acid-functionalized co-delivery micelles with synergistic effect and down-regulation of HIF-1alpha to overcome multidrug resistance. J. Drug Delivery Sci. Technol. 62. https://doi.org/10.1016/j.jddst.2021.102346.

Impey, R.E., Hawkins, D.A., Sutton, J.M., Soares da Costa, T.P., 2020. Overcoming Intrinsic and Acquired Resistance Mechanisms Associated with the Cell Wall of Gram-Negative Bacteria. Antibiotics-Basel 9 (9). https://doi.org/10.3390/antibiotics9090623.

Jiang, T., He, J., Sun, L., Wang, Y., Li, Z., Wang, Q., et al, 2018. Highly efficient photothermal sterilization of water mediated by Prussian blue nanocages. Environ. Sci. Nano 5 (5), 1161–1168. https://doi.org/10.1039/c7en01245d.

Kalan, L., and Wright, G.D.J.E.R.i.M.M. (2011). Antibiotic adjuvants: multicomponent anti-infective strategies. 13(13), -.

Levin, and B., R.J.S. (2001). Why We Don't Get Sick: The Within-Host Population Dynamics of Bacterial Infections. 292(5519), 1112–1115.

Li, J., Liu, X., Tan, L., Cui, Z., Yang, X., Liang, Y., et al, 2019. Zinc-doped Prussian blue enhances photothermal clearance of Staphylococcus aureus and promotes tissue repair in infected wounds. Nat. Commun. 10. https://doi.org/10.1038/s41467-019-12429-6.

Liu, W.-T., Chen, E.-Z., Yang, L., Peng, C., Wang, Q., Xu, Z., et al, 2021. Emerging resistance mechanisms for 4 types of common anti-MRSA antibiotics in Staphylococcus aureus: A comprehensive review. Microb. Pathog. 156, 104915. https://doi.org/10.1016/j.micpath.2021.104915.

Lu, Z., Long, Y., Wang, Y., Wang, X., Xia, C., Li, M., et al, 2021. Phenylboronic acid modified nanoparticles simultaneously target pancreatic cancer and its metastasis and alleviate immunosuppression. Eur. J. Pharm. Biopharm. 165, 164–173. https://doi.org/10.1016/j.ejpb.2021.05.014.

Lubna, M., and Khan, A.U.J.F.i.M. (2016). A Mechanism of Synergistic Effect of Streptomycin and Cefotaxime on CTX-M-15 Type β-lactamase Producing Strain of E. cloacae: A First Report. Front. Microbiol. 7, 2007. 10.3389/fmicb.2016.02007.

Lubna, M., and Khan, A.U.J.F.i.P. (2017). Synergistic Effect of Doripenem and Cefotaxime to Inhibit CTX-M-15 Type β-Lactamases: Biophys. Microbiol. Views. 8, 449-. doi:10.3389/fphar.2017.00449.

Islam S, Redwan A, Millerick K, Filip J, Fan L, Yan W. Effect of Copresence of Zerovalent Iron and Sulfate Reducing Bacteria on Reductive Dechlorination of Trichloroethylene. Environ. Sci. Technol. 55(8), 4851–4861. doi:10.1021/acs.est.0c07702.

Maryam, L., and Khan, A.U.J.I.J.o.B.M. (2018). Combination of aztreonam and cefotaxime against CTX-M-15 type β-lactamases: A mechanism based effective therapeutic approach. Int. J. Biol. Macromol. 1186–1195. 10.1016/j.ijbiomac.2018.05.153.

Maryam, L., Maryam, L., Maryam, L., Khalid, S., Khalid, S., Khalid, S., et al, 2019. Synergistic effect of doripenem in combination with cefoxitin and tetracycline in inhibiting NDM-1 producing bacteria. Future Microbiol. 14 (8), 671–689. https://doi.org/10.2217/fmb-2019-0032.

Mushtaq, S., Warner, M., Williams, G., Critchley, I., Livermore, D. M., 2010. Activity of chequerboard combinations of ceftaroline and NXL104 versus beta-lactamase-producing Enterobacteriaceae. J. Antimicrob. Chemother. 65 (7), 1428–1432. https://doi.org/10.1093/jac/dkq161.

Omollo, C., Singh, V., Kigondu, E., Wasuna, A., Agarwal, P., Moosa, A., et al, 2021. Developing Synergistic Drug Combinations To Restore Antibiotic Sensitivity in Drug-Resistant Mycobacterium tuberculosis. Antimicrob. Agents Chemother. 65 (5). https://doi.org/10.1128/aac.02554-20.

Parvaiz, N., Ahmad, F., Yu, W., MacKerell Jr., A.D., Azam, S.S., 2021. Discovery of beta-lactamase CMY-10 inhibitors for combination therapy against multi-drug resistant Enterobacteriaceae. PLoS ONE 16 (1). https://doi.org/10.1371/journal.pone.0244967.

Pugazhendhi, A., Michael, D., Prakash, D., Krishnamaurthy, P.P., Shanmuganathan, R., Al-Dhabi, N.A., et al, 2020. Antibiogram and plasmid profiling of beta-lactamase producing multi drug resistant Staphylococcus aureus isolated from poultry litter. J. King Saud Univ. Sci. 32 (6), 2723–2727. https://doi.org/10.1016/j.jksus.2020.06.007.

Sharkey, L., and O'Neill, A.J. (2019). *Molecular Mechanisms of Antibiotic Resistance – Part II*. Bacterial Resistance to Antibiotics – From Molecules to Man.

Sondi, I., Salopek-Sondi, B., 2004. Silver nanoparticles as antimicrobial agent: a case study on E-coli as a model for Gram-negative bacteria. J. Colloid Interface Sci. 275 (1), 177–182. https://doi.org/10.1016/j.jcis.2004.02.012.

Srivastava, S., Thomas, T., Howe, D., Malinga, L., Raj, P., Alffenaar, J.-W., et al, 2021. Cefdinir and beta-Lactamase Inhibitor Independent Efficacy Against Mycobacterium tuberculosis. Front. Pharmacol. 12. https://doi.org/10.3389/fphar.2021.677005.

Sun, D., Zhang, W., Mou, Z., Chen, Y., Guo, F., Yang, E., et al, 2017. Transcriptome Analysis Reveals Silver Nanoparticle-Decorated Quercetin Antibacterial Molecular Mechanism. ACS Appl. Mater. Interfaces 9 (11), 10047–10060. https://doi.org/10.1021/acsami.7b02380.

Wang, J.-Q., Wu, J.-Y., Lin, J.-Y., Li, T.-H., Li, D.-F., Gan, N., 2021a. Rapid Detection of Staphylococcus aureus by An Electrochemical Immunosensor Based on Egg Yolk Antibody-Metal Organic Framework Composite Probe. Chin. J. Anal. Chem. 49 (2), 197–206. https://doi.org/10.19756/j.issn.0253-3820.201566.

Wang, X., Tang, H., Wang, C.Z., Zhang, J.L., Wu, W., Jiang, X.Q., 2016. Phenylboronic Acid-Mediated Tumor Targeting of Chitosan Nanoparticles. Theranostics 6 (9), 1378–1392. https://doi.org/10.7150/thno.15156.

Wang, Z., Zhang, P., Ding, X., Wang, J., Sun, D.J.C.E.J., 2021b. Co-Delivery of Ampicillin and β-lactamase Inhibitor by Selenium Nanocomposite to Achieve Synergistic Anti-infective Efficiency through Overcoming Multidrug. Resistance. 414, (1) 128908.

Wei, X., Gao, Y., Hu, Y., Zhang, Y., Zhang, X., 2021. A light-activated nanotherapeutic with broad-spectrum bacterial recognition to eliminate drug-resistant pathogens. J. Mater. Chem. B 9 (5), 1364–1369. https://doi.org/10.1039/d0tb02583f.

Xiu, Z.-M., Zhang, Q.-B., Puppala, H.L., Colvin, V.L., Alvarez, P.J.J., 2012. Negligible Particle-Specific Antibacterial Activity of Silver Nanoparticles. Nano Lett. 12 (8), 4271–4275. https://doi.org/10.1021/nl301934w.

Yao, Z., Zhang, C., Ping, Q.N., Yu, L.L.L., 2007. A series of novel chitosan derivatives: Synthesis, characterization and micellar solubilization of paclitaxel. Carbohydr. Polym. 68 (4), 781–792. https://doi.org/10.1016/j.carbpol.2006.08.023.

Zhang, W., Yu, W., Ding, X., Yin, C., Yan, J., Yang, E., et al, 2019. Self-assembled thermal gold nanorod-loaded thermosensitive liposome-encapsulated ganoderic acid for antibacterial and cancer photochemotherapy. Artif. Cells Nanomed. Biotechnol. 47 (1), 406–419. https://doi.org/10.1080/21691401.2018.1559177.

Zhao, Y., Chen, Z., Chen, Y., Xu, J., Li, J., Jiang, X., 2013. Synergy of Non-antibiotic Drugs and Pyrimidinethiol on Gold Nanoparticles against Superbugs. J. Am. Chem. Soc. 135 (35), 12940–12943. https://doi.org/10.1021/ja4058635.